



Design of air blast pressure sensors based on miniature silicon membrane and piezoresistive gauges

Jérôme Riondet, Anthony Coustou, Hervé Aubert, Patrick Pons, Maylis Lavayssière, Jérôme Luc, Alexandre Lefrançois

► To cite this version:

Jérôme Riondet, Anthony Coustou, Hervé Aubert, Patrick Pons, Maylis Lavayssière, et al.. Design of air blast pressure sensors based on miniature silicon membrane and piezoresistive gauges. Micromechanics and Microsystems Europe Workshop (MME), Aug 2017, Uppsala, Sweden. 6p. hal-01570690

HAL Id: hal-01570690

<https://hal.laas.fr/hal-01570690>

Submitted on 31 Jul 2017

HAL is a multi-disciplinary open access archive for the deposit and dissemination of scientific research documents, whether they are published or not. The documents may come from teaching and research institutions in France or abroad, or from public or private research centers.

L'archive ouverte pluridisciplinaire **HAL**, est destinée au dépôt et à la diffusion de documents scientifiques de niveau recherche, publiés ou non, émanant des établissements d'enseignement et de recherche français ou étrangers, des laboratoires publics ou privés.

Design of air blast pressure sensors based on miniature silicon membrane and piezoresistive gauges

J Riondet^{1,2,3}, A. Coustou^{1,2}, H. Aubert^{1,2}, P. Pons^{1,2}, M. Lavayssière³, J. Luc³, A. Lefrançois³

¹ CNRS-LAAS, 7 Avenue du colonel Roche, F-31400 Toulouse, France

² Université de Toulouse, LAAS-CNRS, F-31400 Toulouse, France

³ CEA-DAM, F-46500 Gramat, France

Corresponding author : ppons@laas.fr

Abstract. Available commercial piezoelectric pressure sensors are not able to accurately reproduce the ultra-fast transient pressure occurring during an air blast experiment. In this communication a new pressure sensor prototype based on a miniature silicon membrane and piezoresistive gauges is reported for significantly improving the performances in terms of time response. Simulation results indicate that it is possible to design a pressure transducer having a fundamental resonant frequency almost ten times greater than the commercial piezoelectric sensors one.

1. Introduction

The typical pressure over time during an explosion is shown in Figure 1 [1-2]. First of all, the pressure increases abruptly (with a rise time between 10 ns and 100 ns) from atmospheric pressure to reach the overpressure peak P_{\max} (several tens of bar depending on the explosive load and the distance from the load). Then the pressure returns back to the atmospheric pressure during a positive phase in 500 μs followed by a negative phase.

In order to validate the hydrocode, i.e. numerical simulations describing the shockwave discontinuity, an accurate measurement of the overpressure peak P_{\max} is required [3], involving the use of pressure sensors presenting a short time response ($\ll 1\mu\text{s}$). Moreover, the high temperature environment during the explosion ($> 1000\text{ }^\circ\text{C}$) makes the real-time dynamic pressure measurement of the blast very challenging.

The sensors used for the dynamic measurement of the pressure in harsh environment are usually piezoelectric pressure sensors (Table 1). Air blast experiments were performed at CEA-Gramat center using many piezoelectric sensors mounted on pencil probes to measure the incident pressure, ie with sensor surface parallel to the shock wave propagation (Figure 2). A typical example of the response of such sensors is illustrated in Figure 3. It can be observed that the time response is too long to provide an accurate estimation of the overpressure peak P_{\max} . The high cut-off frequency of such sensors is approximately 20 % of the resonant frequency. This bandwidth is also degraded by the large dimensions of the sensing part (between 78 mm² and 450 mm²). Moreover typical piezoelectric sensors have a low cut-off frequency ($> 0.5\text{ Hz}$ at -5 %) which is too high to follow the overpressure decrease.

The objective of this work is to achieve a device with a bandwidth at least ten times greater than the bandwidth of the available commercial piezoelectric sensors. In order to overcome the above-mentioned limitations of these sensors, we report here the design of a new piezoresistive pressure sensor based on a silicon membrane and silicon gauges. The piezoresistive detection has been chosen because it provides a better signal-to-noise ratio than their capacitive counterpart [4].

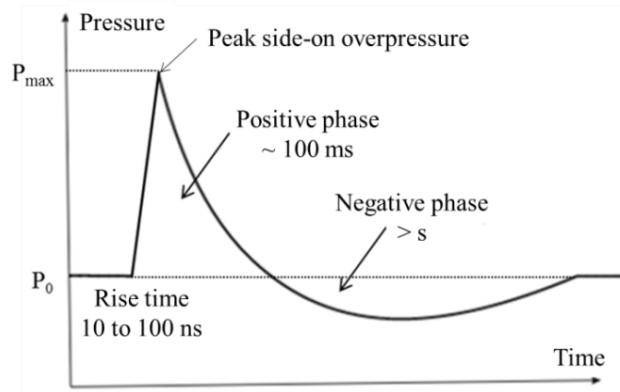


Figure 1: Typical time variation of the pressure during an air blast experiment

Table 1: Characteristics of available commercial piezoelectric sensors used for air blast experiments

Manufacturer	Reference	Pressure range (bar)	Resonant frequency (kHz)
KISTLER	211B5	7.0	300
PCB	113B28	3.5	500
KISTLER	211B4	14	500
PCB	113B24	70	500
PCB	134A34	70	1500

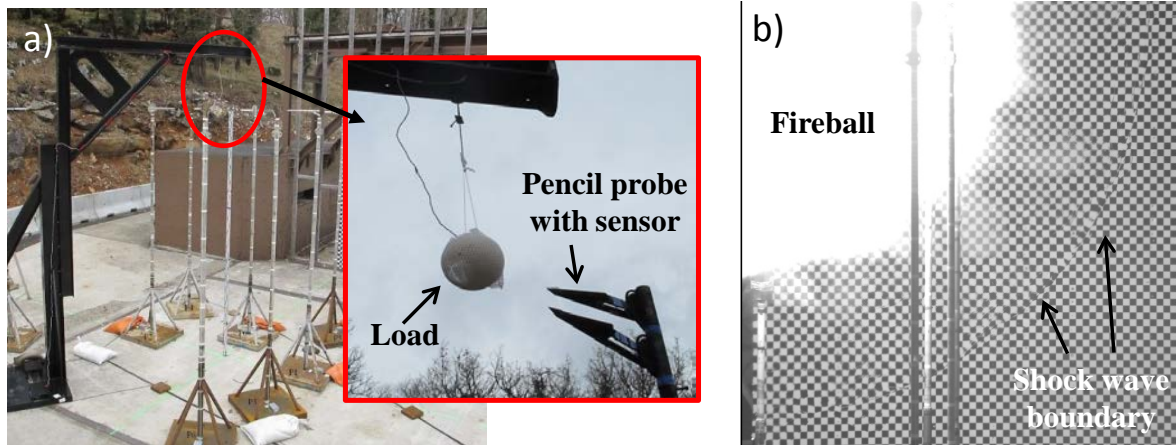


Figure 2: View of air blast experiment: (a) before the explosion and (b) 1.5 ms after the explosion

2. Sensor design

2.1. Sensor topology

The piezoresistive sensor uses here [5] (Figure 4) :

- N-type (100) mono-crystalline silicon membrane with edges parallel to $\langle 110 \rangle$ direction and fabricated from SOI (Silicon On Insulator) wafer;
- P-type silicon gauge obtained from boron implantation. The doping level is of 10^{19} at/cm³ to obtain a good trade-off between the sensitivity of the gauge to the temperature and to stresses. With length-over-width gauge ratio of 5 and for a gauge thickness of 300 nm, the gauge resistance is of few k Ω ;
- A Wheatstone bridge in which the gauges are located close to the edges of a square membrane or at the center of a rectangular membrane (see section 3).

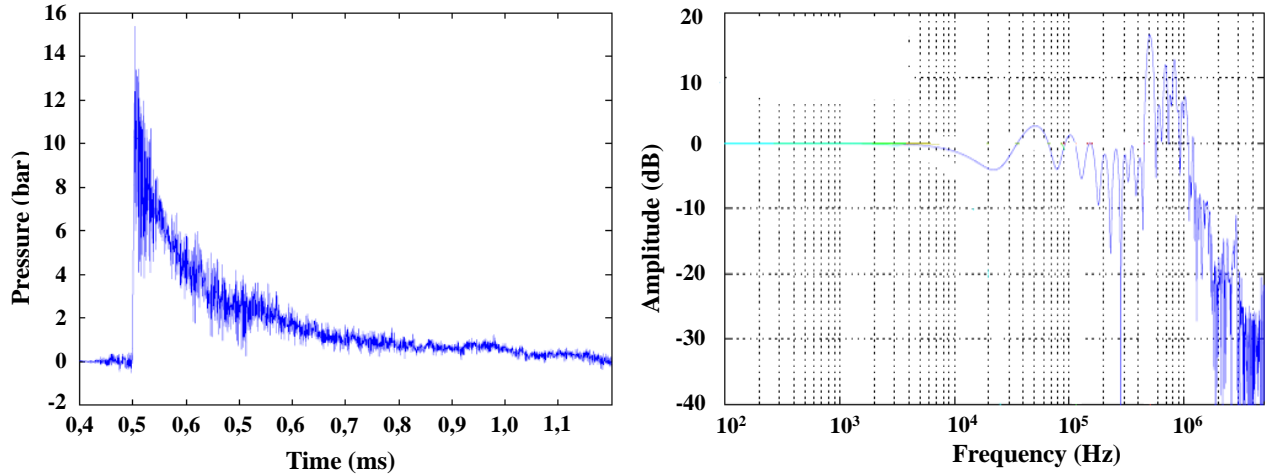


Figure 3. Example of sensor response during air blast experiment (a) time response and b) frequency response.

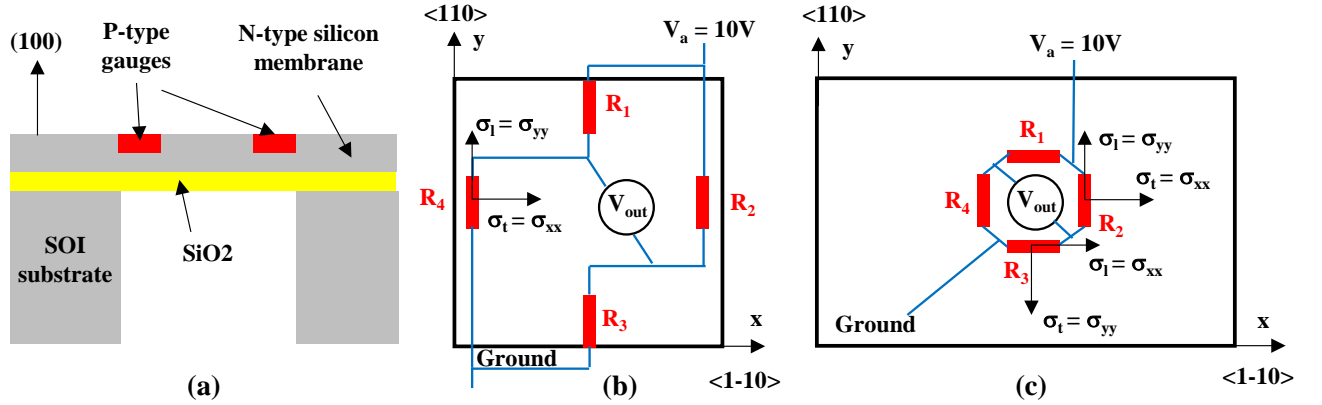


Figure 4: (a) Cross section of the piezoresistive sensor, (b) Wheatstone bridge on a square membrane and (c) Wheatstone bridge on a rectangular membrane

2.2. Mechanical resonant frequency of the piezoresistive sensor

The first design targets the maximization of the mechanical fundamental resonant frequency of the membrane in order to improve the time response of the sensor. For rectangular membrane perfectly clamped at its edges, this frequency F_r is given by equation (1) [6] where E is the Young's modulus, ν is the Poisson ratio, ρ is the membrane mass density, the dimensions e , a and b are respectively the thickness, the width and the length of the membrane and α denotes a coefficient which depends on the ratio b/a (see Table 2). It can be observed that square membrane has a mechanical fundamental resonant frequency almost 60% higher than rectangular membrane with infinite ratio b/a . Moreover rectangular membranes with ratios $b/a > 2$ have a very close resonant frequency. The ratio b/a is then fixed to 3 for stress uniformity considerations as it will be shown in section 3.

The fundamental resonant frequency of square and rectangular ($b/a = 3$) membranes is displayed in Figure 5 versus the membrane width for various membrane thicknesses. The minimum membrane width is here of 20 μm for technological reason (aspect ratio of reactive ionic etching < 20). From these results it can be concluded that it is possible to design a silicon membrane having a mechanical fundamental resonant frequency higher than several tens of MHz.

$$F_r = \alpha * \frac{e}{a^2} * \sqrt{\frac{E}{\rho(1 - \nu^2)}} \quad (1)$$

b/a	1	1.5	2	2.5	3	∞
α	1.66	1.24	1.13	1.09	1.06	1.03

Table 2: Coefficient α as a function of b/a

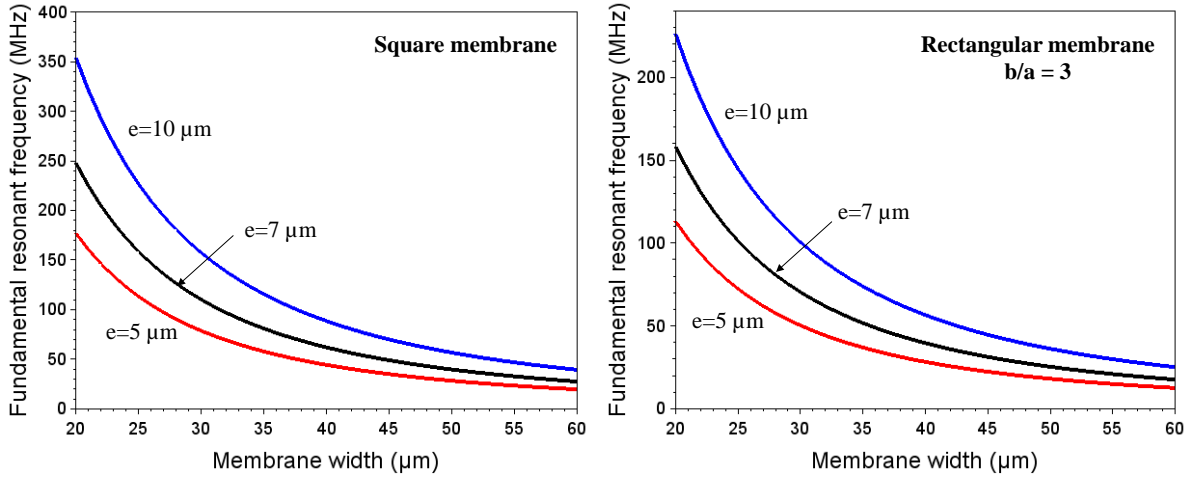


Figure 5: Mechanical fundamental resonant frequency of the membrane as a function of the membrane width for various membrane thicknesses

2.3. Pressure sensitivity

If the four gauges of the Wheatstone bridge have the same initial resistance R_o and the same absolute sensitivity to pressure (i.e., if $\Delta R/R_o = \Delta R_1/R_o = \Delta R_3/R_o = -\Delta R_2/R_o = -\Delta R_4/R_o$), the voltage at the bridge port (V_{out}) can be given by equation (2) [5] where π_{44} is the main piezoresistive coefficient for the chosen configuration ($\pi_{44} \cong 10^{-9} \text{ Pa}^{-1}$ for 10^{19} at/cm^3 P-type doping level) and σ_l (resp., σ_t) is the stress applied to the gauge parallel (resp., perpendicular) to the current flowing in the gauge (see Figure 4). The stress at the membrane surface is given by equation (3) [6], where P is the differential pressure between the two sides of the membrane and σ_n is a coefficient depending on the gauge position on the membrane and on the membrane geometry (Table 3). The sensor response can be derived from equations (2)-(3) and from Table 3 by assuming that the gauges are punctual. Moreover, for the square membrane, we assume that the gauges are located at the centre of the membrane edges and that the stress parallel to the membrane edge is negligible compared to the other stresses. For rectangular membrane it is assumed that the gauges are located at the centre of the membrane and that the stress parallel to the membrane length (along the x-direction) is negligible. Figure 6 gives the sensor response versus the membrane width for different membrane thicknesses and for a differential pressure of 1 bar. It can be observed that, even for the smallest membrane with a thickness of $5\mu\text{m}$, the sensor sensitivity is higher than $0.03\% / \text{bar}$ which is sufficiently high for the targeted application.

$$\frac{V_{out}}{V_a} \cong \frac{\Delta R}{R_o} \cong \frac{\pi_{44}}{2} (\sigma_l - \sigma_t) \quad (2)$$

$$\sigma = \sigma_n * \left(\frac{a}{e}\right)^2 * P \quad (3)$$

Table 3: Coefficient σ_n as a function of the b/a ratio and of the gauge location on the membrane surface

b/a	1	1.4	1.8	≥ 2
Membrane edge (Stress perpendicular to the edge)	0.31	0.44	0.49	0.50
Membrane center (Stress perpendicular to the membrane length)	0.14	0.21	0.24	0.25

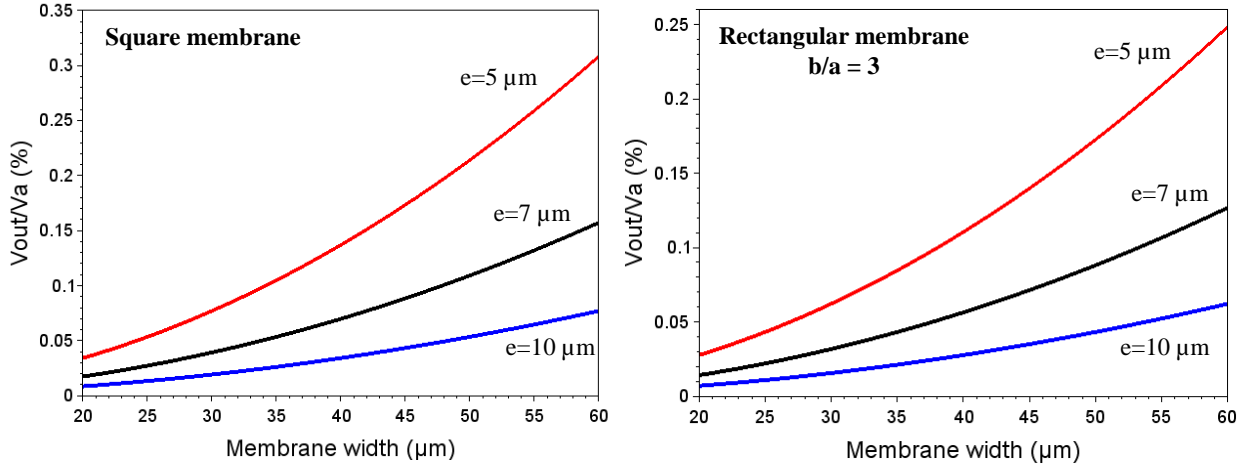


Figure 6: Sensor response versus the membrane width for a differential pressure of 1 bar

2.4. Resolution

At high temperature ($>1000^{\circ}\text{C}$), the electronic noise occurring in the pressure sensor will be dominated by the Johnson noise. In the Wheatstone bridge configuration the unloaded output differential noise voltage V_{bn0} is given by equation (4) where k_b is the Boltzmann constant, T is the absolute temperature, R_0 denotes the initial gauge resistance and Δf the sensor bandwidth. When the sensor is loaded by a $300\ \Omega$ resistor at $T = 1000^{\circ}\text{C}$ while $R_0 = 1\ \text{k}\Omega$ and $\Delta f = 35\ \text{MHz}$, the loaded differential noise voltage V_{bn} is close to $70\ \mu\text{V}$. For a Wheatstone bridge voltage alimentation $V_a = 10\ \text{V}$ and for a full scale response $[V_{out}/V_a]_{FullScale} = 1\%$, the resolution is then better than 0.1% of the full scale range.

$$V_{bn0} = 2\sqrt{4k_bTR_0\Delta f} \quad (4)$$

3. Sensor modelling

The sensors with perfectly clamped square and rectangular membranes were simulated using COMSOL software (Figure 7). The gauges were modelled by a $300\ \text{nm}$ -thick P-type ($10^{19}\text{at}/\text{cm}^3$) monocrystalline silicon and the interconnection by $5\ \mu\text{m}$ -thick P-type ($10^{20}\text{at}/\text{cm}^3$) monocrystalline silicon. To obtain a good trade-off between the mechanical resonant frequency and pressure sensitivity values, the width of the square (respectively rectangular) membrane is fixed to $40\ \mu\text{m}$ (respectively $30\ \mu\text{m}$). For the square membrane, the four gauges are not located exactly at the membrane edges in order to minimize the impact of eventual misalignment between gauges and the membrane. For the rectangular membrane, the gauge location is constrained by the gauge length.

The stress distribution ($\sigma_{xx} - \sigma_{yy}$) is shown in Figure 8 for square and rectangular membranes and for differential pressure of 1 bar. For square membrane, it can be observed a fast variation of stress along the x and y directions while for rectangular membrane, the stress distribution is quite uniform on the gauge surface, allowing more flexibility against misalignment error between the gauges and membrane. Within these stress distributions, the sensor responses were calculated using Multiphysics COMSOL software. Table 4 summarized the sensors performances for the square and rectangular membranes. The resonant frequency reached values between $30\ \text{MHz}$ and $40\ \text{MHz}$ and the sensitivity is of $0.05\ \%/ \text{bar}$.

4. Conclusion

A miniaturized piezoresistive pressure sensor has been designed to overcome the limitations of available commercial piezoelectric sensors used for the monitoring of the dynamic pressure during air blast experiments. Modelling and simulation results show that it is possible to design sensors with a time response significantly improved compared to the state-of-the-art.

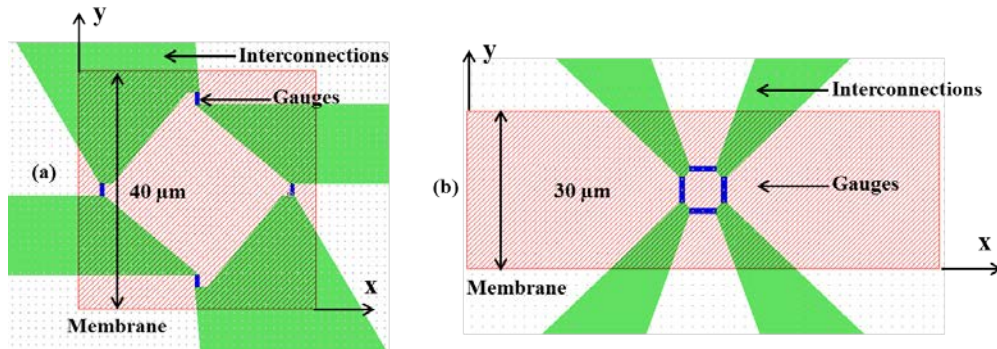


Figure 7: Sensor configurations simulated with COMSOL software with (a) a square membrane and (b) a rectangular membrane

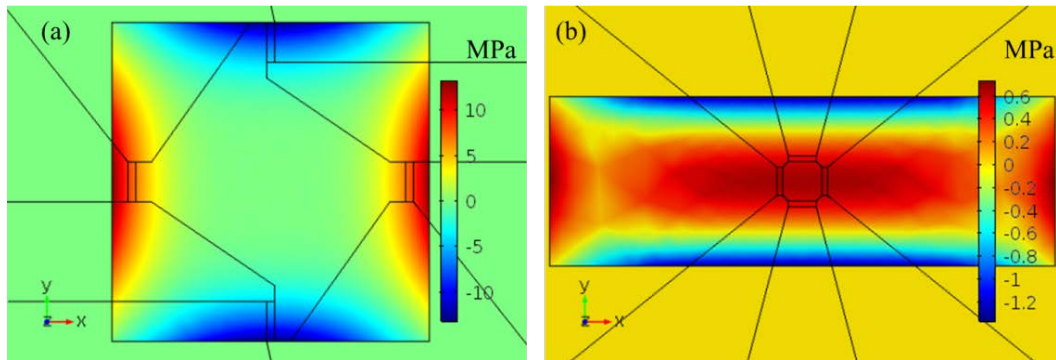


Figure 8: Stress ($\sigma_{xx} - \sigma_{yy}$) for a differential pressure of 1bar with (a) a square membrane and (b) a rectangular membrane

Table 4: Sensor dimensions and simulated performances

	Membrane thickness	Membrane Width Length	Gauge Width Length	Resonant frequency from Eq. (1)	Resonant frequency from COMSOL	Sensitivity from Eq. (2)	Sensitivity from COMSOL
Square membrane	5 μm	40 μm 40 μm	1 μm 5 μm	45 MHz	30 MHz	0.13% / bar	0.05% / bar
Rectangular membrane	5 μm	30 μm 90 μm	1 μm 5 μm	50 MHz	42 MHz	0.06% / bar	0.04% / bar

Acknowledgements

This work was partially funded by Occitanie Region through the COCNANO project.

References

- [1] W. Fickett, C. William, Detonation: Theory and Experiment, Dover Publications, 2011.
- [2] P.-L. Walter, Air-blast and the Science of Dynamic Pressure Measurements, Sound and Vibration, pp. 10-16, December 2004.
- [3] P. L. Silver, Evaluation of Air Blast Measurement Techniques, 75th Shock and Vibration Proceedings, Virginia Beach, VA, October 17 - 22, 2004.
- [4] E. Mile, Nanowire and carbon nanotube based NEMS resonator, PhD Thesis, June 2010
- [5] M. Olszacki, Modeling and optimization of piezoresistive pressure sensors, PhD Thesis, July 2009
- [6] R. J. Roark, W. C. Young, et R. G. Budynas, Roark's formulas for stress and strain, 7th ed. New York: McGraw-Hill, 2002